Floquet spectroscopy of hydrogenic states: Classical and quantal descriptions

Y. Zhang, M. Ciocca, L.-W. He, C. E. Burkhardt, and J. J. Leventhal
Department of Physics, University of Missouri–St. Louis, St. Louis, Missouri 63121
(Received 14 February 1994; revised manuscript received 2 May 1994)

The responses of hydrogenic states of highly excited Rydberg atoms to dc and rf electric fields have been studied and the data interpreted from both classical and quantal viewpoints. The solution of the Schrödinger equation for this system leads to a network of progenitor and sideband states, a Floquet-Stark map that, although complex, exhibits regularities. These regularities are interpreted from a classical viewpoint by considering the near-Keplerian orbit of the valence electron as the dynamical entity rather than the electron itself. It is shown that the regularities in the Floquet-Stark map are the result of a commensurability of the dc Stark frequency and that of the applied rf. The experimental technique employed, Floquet spectroscopy, also provides data from which atomic parameters may be extracted, in this case the quantum of the (permanent) electric dipole moment (QDM) associated with hydrogenic manifolds of sodium Rydberg atoms. It is observed that the QDM's for sodium are larger than those for corresponding states of hydrogen. This observation is interpreted from a classical point of view.

PACS number(s): 32.30.Bv, 32.60.+i, 32.80.−t

INTRODUCTION

Although the ac Stark effect was first studied in 1955 [1], the availability of the laser as an experimental tool has led to a rebirth of interest in this phenomenon. On the one hand, high-power lasers make it possible to subject atoms in low-lying states to intense ac fields [2]. On the other hand, lasers may be used to produce atoms in high-lying Rydberg states, states for which the fields produced by ordinary laboratory microwave or rf, generators are effectively "intense" [3,4]. Moreover, Rydberg atoms provide the opportunity to investigate atomic properties under conditions in which aspects of both quantal and classical descriptions of the system may be valid [5–9]. As a consequence, correlations between quantum-mechanical and classical mechanical descriptions may reveal themselves. Such correlations can be helpful for understanding the underlying principles. Further, a classical description permits visualization of the atomic properties, a feature that is particularly useful when examining the responses of atoms to external fields.

The goal of the work presented here is to examine these correlations for the responses of hydrogenic states, states with very small quantum defects, of highly excited Rydberg atoms to dc and ac electric fields. We do this by comparing the results of experiments in which these fields are applied to state-selected Rydberg atoms with predictions based on the quantal and classical descriptions. We refer to the experimental technique as Floquet spectroscopy. The data are in the form of spectra that reflect the nature of the complex energy-level diagram that arises from simultaneous application of the dc and ac fields.

The quantum-mechanical description is straightforward. The time-dependent Schrödinger equation is solved with the aid of the Floquet theorem and the energy-level structure thus obtained. To describe the system classically we use the fact that, in our experiments, the ac field is of radio frequency (rf) and is therefore much lower than the classical electronic orbital frequency. The nature of the atomic responses can thus be understood by considering the electronic orbit, rather than the electron itself, as the dynamical entry. This leads to a picture of the waferlike electronic orbit, rotating and pulsating in response to the applied electric fields. The equations of motion of this rotating orbit are integrable and clearly show the conditions under which periodic motion can occur. The nature of the trajectory of this system in phase space, in conjunction with the Bohr-Sommerfeld quantization condition and the correspondence principle, then leads to an energy-level diagram that is consistent with that obtained quantum mechanically.

It is interesting to contrast these rf experiments with those in which highly excited hydrogen atoms are subjected to a microwave field, the frequency of which is ~20–100 times the rf frequencies employed here. For most of the microwave work, treatment of the electronic orbit would be inappropriate because the orbital and microwave frequencies are comparable [3,10,11]. The important effect that has been observed in the microwave work is the rapid and nearly complete multiphoton ionization of the hydrogen atoms for field strengths exceeding some critical value. This phenomenon has been attributed to a transition of the system from ordered to chaotic behavior, a transition that is possible because the equations of motion are not integrable. If, however, the orbit can be treated as the dynamical entity, the resulting equations *are* integrable and chaotic motion cannot ensue. Consistent with this premise, runaway multiphoton ionization of sodium Rydberg atoms was not observed for the rf field strengths used in these experiments.

APPARATUS

The experiments were conducted using apparatus designed for precision Stark spectroscopy [12]. A beam of sodium atoms was irradiated with three laser beams at

the center of a pair of Stark plates located inside a stainless-steel cell that provided electrostatic shielding. The atomic beam, density $\sim 10^7$ cm^{-3}, was produced in an effusive oven located beneath the cell. The dc and rf fields were applied to the Stark plates; both fields were perpendicular to the plates in these experiments. The beams from two 10-Hz pulsed grazing-incidence dye lasers pumped by a single Nd:YAG laser (where YAG denotes yttrium aluminum garnet) were used to excite the atoms to an intermediate state $10d\ ^2D$ or $12s\ ^2S$ via Na($3p\ ^2P$). The third laser, a cw line-selectable CO_2 laser, placed the energy of the system, excluding that of the electric fields, ~ 1000 cm^{-1} above the intermediate state. The narrow bandwidth of the CO_2 laser line, ~ 50 kHz, permitted selective excitation in the region of the closely packed states for $n \approx 64$. Since the energy of photons of the CO_2 laser lines is fixed, this energy is not, in general, resonant for excitation from the intermediate state to a higher bound state. Application of a dc electric field F was used to Stark shift the higher states into resonance.

The value of F was therefore set prior to each laser pulse. It was increased about 5 μs after the pulses, which were ~ 7 ns duration, to ~ 100 V/cm, sufficient to ionize highly excited atoms, but not atoms in the intermediate states. Thus ions resulting from field ionization served to signify absorption of photons from all three laser beams. The Stark plates were designed to produce uniform fields as discussed previously [12–14]. One plate contained a slit 2.5 cm long by 500 μm wide to permit passage of the ions from the excitation region and into the detection region. These ions were electrostatically focused and detected with a CuBe particle multiplier using a charge-sensitive amplifier.

Data were obtained with fixed laser wavelengths, rf amplitude G and rf frequency ω_0. F was varied stepwise and the ion signal measured at each setting. F spectra were thus assembled using, typically, 100 laser shots per field setting. The method by which F spectra were assembled is illustrated in Fig. 1, which is a conventional Stark map for hydrogen [15]; for clarity it is assumed that $G=0$ in the figure. The horizontal line represents the energy of the intermediate state plus that of a photon in the particular CO_2 laser line being used. This energy, which we refer to as the three-photon energy, is that available for atomic excitation, not including the energy of any rf photons for cases for which $G \neq 0$. The slanted lines are the dc Stark states emanating from the zero-field (degenerate) energy of hydrogen with a given principal quantum number. Excitations can occur when the energy of the Stark states matches the three-photon energy, i.e., at intersections of the slanted lines with the horizontal line. Note that the resolution for adjacent states increases with increasing F. Symmetric scans of F, positive to negative, were employed in order to determine the nominal zero-field value and negate inaccuracies introduced by any offset. In any case, this offset was typically 30 mV/cm, but never exceeded 80 mV/cm [12].

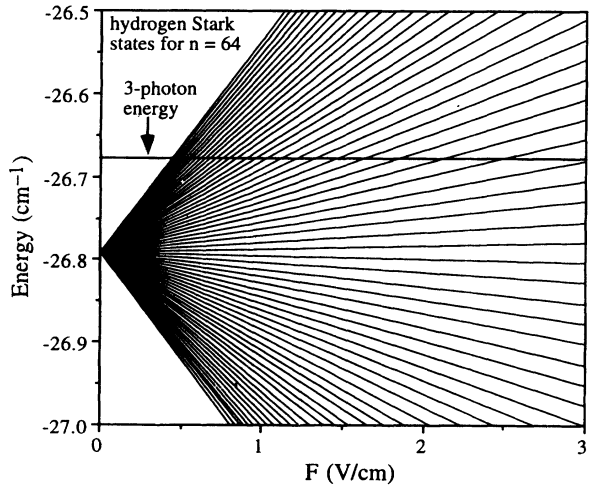

FIG. 1. Energy-level diagram for the $n=64$ manifold of hydrogen Stark states. The line representing the three-photon energy is arbitrarily placed. The figure illustrates the method by which F spectra are assembled. For clarity it is assumed that $G=0$. The three-photon energy is the total energy available for excitation which can occur only at intersections with the Stark states. F-spectra, ion signal vs F, thus exhibit peaks at these intersections.

QUANTUM-MECHANICAL DESCRIPTION

The Hamiltonian of the system may be written in the form

$$H = H_a + H_S \ , \tag{1}$$

where H_a is the atomic Hamiltonian and H_S contains the external fields. Since excited states of hydrogen or states that constitute the hydrogenic manifolds of Rydberg atoms may possess a permanent electric dipole moment, H_S is given, in the electric dipole approximation, by

$$H_S = -\mathbf{p}\cdot\mathcal{E} \ , \tag{2}$$

where p is the permanent electric dipole moment and

$$\mathcal{E} = \mathbf{F} + \mathbf{G}\cos(\omega_0 t) \tag{3}$$

is the applied electric field. If $\mathbf{F}$ and $\mathbf{G}$ are in the z direction, $\mathbf{H}_S$ is given by

$$H_S = -p_z[F + G\cos(\omega_0 t)] \ , \tag{4}$$

where p_z is the z component of $\mathbf{p}$. The time-independent term in H_S, $p_z F$, leads to the dc Stark effect, which, in this case, is the *linear* dc Stark effect. Applying the Floquet theorem [16], we find that the sinusoidal term in H_S produces a ladder of equally spaced quasienergy states, Floquet states, separated by $\hbar\omega_0$ and centered at the energy of the original degenerate level, the progenitor level, as illustrated in Fig. 2. Figure 2(a) shows the field-free level and Fig. 2(b) the ladder of the states that arises when $F=0$ and $G \neq 0$.

If $G=0$ and $F \neq 0$ we have the familiar linear Stark map of the splitting of the (field-free) degenerate level, Fig. 2(c). At any given nonzero value of F, a vertical line in this figure, there exists a set of dc Stark states separated by

$$[\Delta E_S \text{ (in MHz)}]=3.84[F \text{ (in V/cm)}]n \ , \tag{5}$$

where n is the principal quantum number. Thus principal quantum numbers in the range 40–70 require fields of only ~ 1 V/cm to make ΔE_S comparable with the energy of rf photons.

Application of the sinusoidal field produces a ladder of Floquet states associated with *each* of the dc Stark states. Changing F produces a different dc Stark state, but each such state becomes a progenitor (carrier) for an array of Floquet states (sidebands). The separation between sideband states in a given array is $\hbar\omega_0$. The energy-level structure that arises from simultaneous application of dc and ac fields is illustrated in the Floquet-Stark diagram shown in Fig. 2(d). Only two Floquet states on each side of the ($F=0$) progenitor are included in the diagram, but each of these $F=0$ states produces a fan of states as F is turned on, as in Fig. 2(c). Thus the partial lifting of the hydrogenic degeneracy by the dc field, together with the sideband states produced by application of the ac field, leads to a complicated network of levels.

The number of sideband states that are important in a given experiment, i.e., the number that must be included in the diagram, depends upon the amplitude G of the ac field [17]. That is, the probability of a transition to a particular Floquet sideband depends upon the ac amplitude. The solution of the time-dependent Schrödinger equation with $\Psi(\mathbf{r},t)=R(\mathbf{r})\phi(t)$ shows that $R(\mathbf{r})$ is identical to the spatial part of the solution of the Schrödinger equation using only the time-independent part of the Hamiltonian, i.e., H_a plus the first term in Eq. (4) [11]. $\phi(t)$ is given by

$$\phi(t)=\exp\left[-\frac{\imath}{\hbar}(E_a-p_zF)\right] \times\exp\left[\imath\left[\frac{p_zG}{\hbar\omega}\right]\sin(\omega_0 t)\right] , \tag{6}$$

where E_a is the field-free energy of the degenerate levels. The first exponential in Eq. (6) is the time dependence associated with the dc Stark energies; the second, which arises from application of the ac field, may be expanded as a Fourier series [18]

$$\exp\left[\imath\left[\frac{p_zG}{\hbar\omega_0}\right]\sin(\omega_0 t)\right]=\sum_{\mathcal{K}=-\infty}^{\infty} J_{\mathcal{K}}\left[\frac{p_zG}{\hbar\omega_0}\right]\exp[\imath(\mathcal{K}\omega_0 t)] =\sum_{\mathcal{K}=-\infty}^{\infty} C_{\mathcal{K}}\exp[\imath(\mathcal{K}\omega_0 t)] , \tag{7}$$

where the $J_{\mathcal{K}}$ are Bessel functions of the first kind of integral order $\mathcal{K}$. This expansion clearly shows that the quasienergy states, the Floquet states, resulting from application of the ac field have energies given by

$$E_{n,\mathcal{K}}=E_a-p_zF+\mathcal{K}\hbar\omega_0, \quad \mathcal{K}=0,\pm1,\pm2,\ldots . \tag{8}$$

Moreover, since the spatial part of the wave function is the same for all Floquet states,

$$|C_{\mathcal{K}}|^2=\left|J_{\mathcal{K}}\left[\frac{p_zG}{\hbar\omega_0}\right]\right|^2 \tag{9}$$

is a measure of the relative probability for absorption

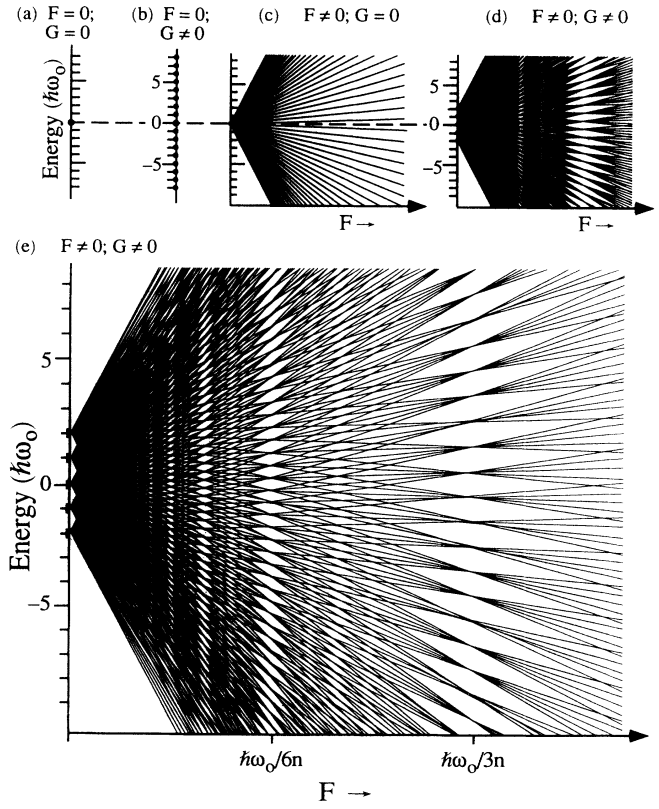

FIG. 2. Schematic energy-level diagram showing the splitting of a degenerate hydrogenic state under application of dc and ac electric fields for the cases indicated; (e) is an enlarged version of (d) to show detail. F is in a.u. provided $\hbar\omega_0$ is in a.u. The dashed line though the degenerate field-free progenitor states in (a)–(d) emphasizes the fact that these states do not shift energy upon application of the ac field.

provided, as is the case here, that these low fields have virtually no effect on the intermediate state. Moreover, this formulation, and therefore Eq. (9), is only valid for the linear Stark effect. That is, Eq. (9) is only applicable when F is low enough so that p_z is independent of F. In these experiments Eq. (9) is expected to be valid, so that our F spectra should reflect the magnitudes of the $|C_{\ell}|^2$ at each sideband. Since, however, the Bessel functions oscillate, their values depending on both p_z and G, the probability amplitudes $|C_{\ell}|^2$ will not be simply related. Therefore, the absorption strengths of the sidebands associated with a given progenitor are not simply related. This feature of the spectra if not, of course, included in the density of states diagram Figs. 2(d) and 2(e). Data illustrating this aspect of Floquet spectroscopy will be presented later in this paper.

Despite the complicated nature of Figs. 2(d) and 2(e), there are some regularities, the most obvious of which are the spaces in the density of states at certain values of the static field F. The shapes of the diamondlike gaps, however, depend upon the number of Floquet states included in the diagram. As this number is increased, the width in F decreases. In the limit for which it is necessary to include a large number of sidebands, corresponding to large G, the width of the gaps shrinks to zero. This structure can be probed using Floquet spectroscopy [19].

CLASSICAL DESCRIPTION

In the absence of external fields, the force on the Rydberg electron is a $1/r^2$ attraction to the nucleus plus a small central field perturbation from higher-order interactions such as polarization of the ionic core by the Rydberg electron [20,21]. The perturbation causes the otherwise Keplerian orbit to process about the force center. The motion is still, however, confined to a plane. The Keplerian frequency is given by $1/(2\pi n^3)$ in a.u., which, consistent with the correspondence principle, is also the separation between adjacent quantum states in field-free hydrogen. For $n=50$ the orbital period is ~ 0.5 ps; the period of a 500-MHz field is 20 ns. The electron therefore executes $\sim(4\times 10^4)$ elliptical orbits during each rf cycle, justifying treating the orbit as the dynamical entity. This is simply another way of stating that the separation between adjacent n states is much greater than the energy of a single rf photon. This condition is the antithesis of that encountered in most of the microwave work, although recent experiments have been performed in which the separation between adjacent states is ~ 50 microwave photons [22,23].

When a constant dc electric field is applied to a hydrogen atom or a multielectron atom in a hydrogenic Rydberg state, angular momentum is no longer conserved and the plane of the electronic motion rotates about the electric-field vector with constant angular frequency $\omega_S=\frac{3}{2}nF$ rad/atu (1 atu$=2.42\times 10^{-17}$s) [24]. Simultaneously, the semiminor axis pulsates, but the length of the major axis remains fixed. If the orbital precession resulting from interactions with the core of the Rydberg atom is much faster than the rotation about F, the charge distribution is, on average, symmetric and the Rydberg state has no effective dipole moment. Therefore, in contrast to the case of excited hydrogen atoms, the quadratic Stark effect will be observed at low dc fields for *all* Rydberg states. For the most hydrogenic Rydberg states, states for which the quantum defect is very small, the "low dc field" is indeed very low. Nevertheless, all multielectron Rydberg atoms undergo a quadratic Stark shift as F is turned on. For higher values of F, ω_S can be much greater than the core-induced precession and the nearly Keplerian orbit rotates about F many times before completing one precessional cycle. In this case the elliptical orbit provides a permanent electric dipole moment and the linear Stark effect is observed. The classical and quantum regimes are linked by the correspondence principle, according to which the splitting between adjacent Stark levels is equal to $\hbar\omega_S$. Note that ω_S in MHz is then equal to ΔE_S in Eq. (5).

Now, the Hamiltonian for a permanent electric dipole in a dc field $\mathbf{F}=F\mathbf{k}$ is given by

$$\begin{aligned} H_S &= -\mathbf{p}\cdot\mathbf{F} \\ &= -p_z F \\ &= -(3/2)n^2 A_z F \\ &= -\omega_S A_z \ , \end{aligned} \tag{10}$$

where A_z is the z component of the Lenz vector $\mathbf{A}$. Since A_z is conserved, i.e., its conjugate angle Ω does not appear in the Hamiltonian, it may be identified with the action I. Letting $I=-A_z$ we have [25]

$$H_S=\omega_S I \ . \tag{11}$$

We note that this Hamiltonian has the same form as that of a harmonic oscillator, viz., a constant times the first power of the action. Applying Hamilton's equations we see that the frequency associated with the angle variable conjugate to I is a constant. Classically this means that the frequency is independent of the energy, just as for a harmonic oscillator. Application of the correspondence principle shows that the separation between adjacent states is a constant [see Eq. (5)] $\hbar\omega_S$, as for the harmonic oscillator.

In these experiments $\mathbf{G}$ and $\mathbf{F}$ are parallel, $\mathbf{G}=G\mathbf{k}$, so we need only replace F in the above equations by $F+G\cos(\omega_0 t)$ and obtain

$$H_S=\omega_S I+\gamma I\cos(\omega_0 t) \ , \tag{12}$$

where $\gamma=\frac{3}{2}n^2 G$. Since the coefficient of the periodic term contains only I and not its conjugate coordinate, I remains a conserved quantity, i.e., it is still an action. The action angle Ω conjugate to I is given by one of Hamilton's equations

$$\dot{\Omega}=\frac{\partial H_S}{\partial I}=\omega_S+\gamma\cos(\omega_0 t) \ , \tag{13}$$

so that

$$\Omega=\omega_S t+\frac{\gamma}{\omega_0}\sin(\omega_0 t) \ . \tag{14}$$

Making the substitution $\theta=\omega_0 t$, we have

$$\Omega=\left[\frac{\omega_S}{\omega_0}\right]\theta+\left[\frac{\gamma}{\omega_0}\right]\sin\theta\ . \tag{15}$$

This equation represents the trajectory in phase space of the system for specified values of ω_S (specified by n and F) and ω_0 (specified by the setting on the rf generator). This trajectory is conveniently plotted on a torus with Ω as the azimuthal angle and θ the angular position of the trajectory on the circular cross section of the torus [26]. Since θ must be taken mod2π, the first term is periodic with period $2\pi(\omega_0/\omega_S)$; the period of the second term is obviously 2π. Thus the *system*, i.e., the variable Ω, can exhibit periodic behavior only if the ratio (ω_0/ω_S) is a rational number, that is, if ω_S and ω_0 are commensurate. Of course Ω must also be taken mod2π.

Figure 3 shows trajectories in phase space for four different values of (ω_0,ω_S). If the ratio (ω_0/ω_S) is rational and greater than unity, then the trajectory will wind around the torus more than once in one circuit of Ω, i.e., θ has traversed integral multiples of 2π when $\Omega=2\pi$. The torus and such a path in phase space resemble a toroidal solenoid. For example, if $(\omega_0/\omega_S)=2$ [Fig. 3(b)], then the period of the system is 4π (in θ). If, however, (ω_0/ω_S) is rational but less than unity, the trajectory must traverse the ring of the torus more than once before returning to the initial point as in Fig. 3(c).

If (ω_0/ω_S) is irrational, then the system will exhibit quasiperiodic behavior, with no intrinsic period. The trajectory in phase space will, after a sufficient number of Ω circuits, cover the entire surface of the torus. Note that if the ratio is rational, but say 1000/1001, the period will be very long, i.e., it will take many Ω circuits for the system to return to the initial point, 1001 for this case. A portion of such a trajectory is illustrated in Fig. 3(d).

By examining the nature of the trajectory in phase space and applying the Bohr-Sommerfeld quantization condition together with the correspondence principle we can construct a semiclassical energy-level diagram for the system. According to the correspondence principle, the separation between adjacent quantum states is $\hbar\omega$, where ω is the frequency of the system, if indeed the system is periodic. If it is not, i.e., if it is quasiperiodic, then the energy levels form a continuum. As discussed above, when the rf and dc Stark frequencies are commensurate, the trajectory on the torus is periodic, as is the system. Moreover, the period is independent of the rf amplitude, and therefore the energy, so that a ladder of states, separated by $\hbar\omega$, results. This ladder of equally spaced states is comparable with the case of the harmonic oscillator or the dc Stark effect on excited-state hydrogen (the linear Stark effect), both of which have Hamiltonians equal to the action times the system frequency. Equation (8) is of similar form, but as discussed above, the motion is periodic only if the rf and dc Stark frequencies are commensurate; otherwise it is quasiperiodic.

Figure 4 is a semiclassical energy-level diagram constructed as discussed above. Ladders of levels are shown at several rational values of the ratio ω_S/ω_0. Also illustrated are the continua of levels at irrational values of ω_S/ω_0, values for which the trajectories in phase space are quasiperiodic. Omitted from the diagram for clarity are the ladders of levels at rational values of ω_S/ω_0, but for which the periods in phase space are very long, i.e., quantum ladders with very small spacings between adjacent states.

Since the abscissa in Fig. 4 is ω_S/ω_0, and $\omega_S=\frac{3}{2}nF$, this diagram may be compared to the quantum-mechanical diagram shown in Figs. 2(d) and 2(e). It can

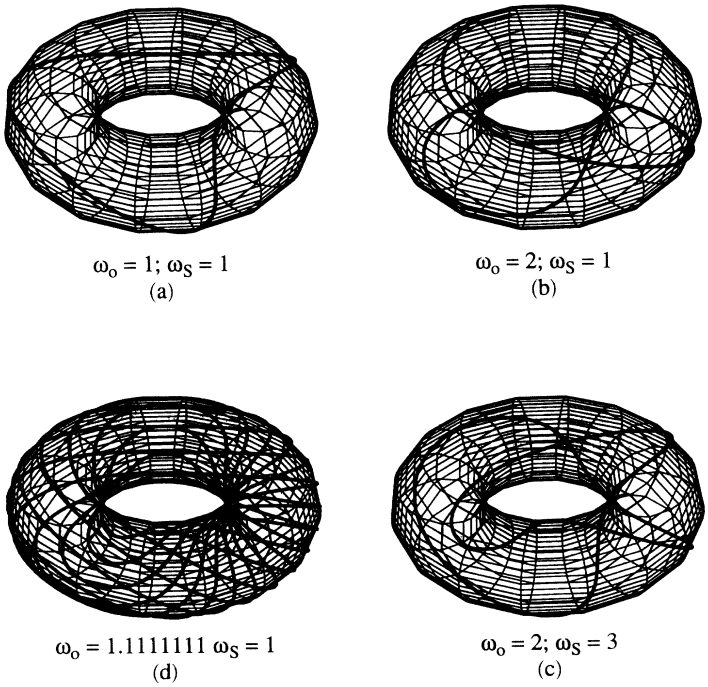

FIG. 3. Trajectories in phase space for the values of ω_0/ω_S indicated. The trajectory in (d) shows a few Ω circuits and illustrates the case for which the ratio ω_0/ω_S is irrational, or nearly so (see text).

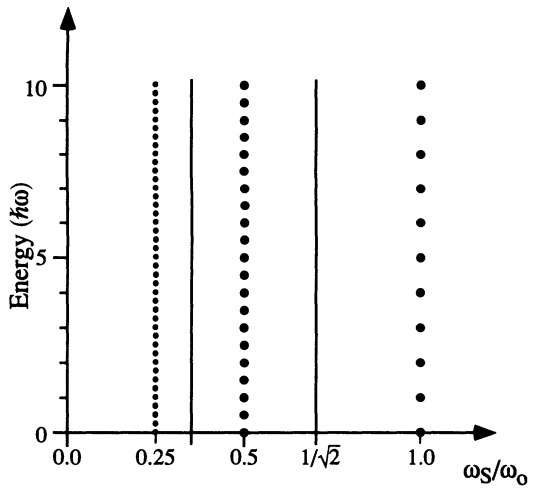

FIG. 4. Semiclassical energy-level diagram constructed using the correspondence principle as described in the text.

be seen that the gaps that occur in the quantum diagram coincide with the ladders of levels at rational values of ω_S/ω_0 in the semiclassical diagram. When making this comparison it must be borne in mind that the quantum diagram was constructed with only two sideband states on each side of the carrier so the gaps are obvious. Had more sidebands been included, the gaps would be narrower in the horizontal direction, but the vertical (energy) spacing would be unchanged. In the limit of a great many sideband states the gaps would be quite narrow, taking on the appearance of a complete semiclassical diagram.

Figure 2(e) clearly shows that there are smaller gaps near the major gaps in the quantum-mechanical diagram. These correspond to rational frequency ratios having long phase-space periods, i.e., low system frequencies. They therefore consist of a great many closely spaced levels that are not resolvable in our experiment. Notice that in both the quantal and classical formulations the time-dependent systems have been converted to equivalent time-independent systems. In the quantal case this was accomplished by application of Floquet's theorem. The classical conversion was effected by a canonical transformation [27].

RESULTS AND DISCUSSION

We wish to measure atomic parameters for hydrogenic states of sodium Rydberg atoms and to compare these parameters with those of analogous states of hydrogen. This provides information on the effects of the Rydberg atom core. It also permits assessment of the degree to which hydrogenic states of Rydberg atoms may be treated as states of hydrogen. We know, for example, that at very low dc fields the hydrogenic states are not hydrogenic at all. That is, they exhibit a quadratic Stark effect because they are not truly degenerate [21]. We also know that, at relatively high values of F, blue Stark states (those that shift to higher energy upon application of F) of a given hydrogenic manifold overlap with red states of the manifold of the next higher principal quantum number. Avoided crossings then lead to a tangled network of commingled states [15], the so-called region of spaghetti [15]. In contrast, analogous Stark states of hydrogen atoms do indeed cross so that the region of spaghetti is decidedly nonhydrogenic. Since we wish to examine the behavior of hydrogenic states we focus on $F<1/(3n^5)$, in a.u., at which value the bluest n Stark state coincides with the reddest $(n+1)$ Stark state; for $n=64$, $1/(3n^5)<1.6$ V/cm.

There are two characteristics of the dc Stark effect in hydrogen that may be considered the criteria that define hydrogenic behavior. First, the linear Stark effect must be observed. Second, the spacings ΔE_S between adjacent Stark states of the same hydrogenic manifold must be the same, or very nearly so, for fixed F [see Eq. (5) for ΔE_S in hydrogen]. That is, the Hamiltonian is equal to the action times the frequency, ω_S in this case. Thus the z component of the permanent electric dipole moment is quantized, which is equivalent to noting that the z component of the Lenz vector is quantized [15]. For hydrogen the quantum of p_z in a.u. is $3n$.

In actuality, of course, ΔE_S, and consequently ω_S, cannot be truly constant over the entire manifold for any multielectron atom because each zero-field angular momentum state corresponds to a different *effective* principal quantum number, n^*, given by

$$n^*=n-\delta_l \ , \tag{16}$$

where δ_l is the l-dependent quantum defect. In sodium the quantum defects are very nearly zero for $l\geq 2$ so that ω_S should be nearly constant over the hydrogenic manifold. In general, however, the value of ω_S, and hence p_z, will not be the same as for hydrogen. The differences are slight, but our experimental technique is sensitive enough to detect them. We can therefore examine the extent to which the hydrogenic manifolds of sodium behave as states of hydrogen. Moreover, we can measure the quantum of p_z for sodium.

We begin with an F spectrum acquired with no applied rf. Figure 5(a) shows such a spectrum for the blue states of the $n=64$ hydrogenic manifold of sodium. This spectrum has been placed on a Stark map of hydrogen states with the base line at the three-photon energy. The triangles are the positions of the intersections of the hydrogen Stark states with a horizontal line (not shown) at the total excitation energy. Thus the triangles represent the expected locations of the peaks if these were dc Stark states of hydrogen. While there appears to be reasonable agreement between the positions of the peaks and the triangles at low values of F, the disparity increases at higher values. This is a consequence of the inherently higher resolution of the experiment at higher fields because, at constant energy, the horizontal separations between adjacent Stark states increases with increasing F.

Now, the Stark shift in hydrogen is given by

$$E_S(n_1,n_2,F)=\tfrac{3}{2}n(n_1-n_2)F=\tfrac{3}{2}nkF \ , \tag{17}$$

where n_1 and n_2 are parabolic quantum numbers and $k=n_1-n_2$ is the electric quantum number which changes in increments of 2 [15]. The coefficient of F is p_z,

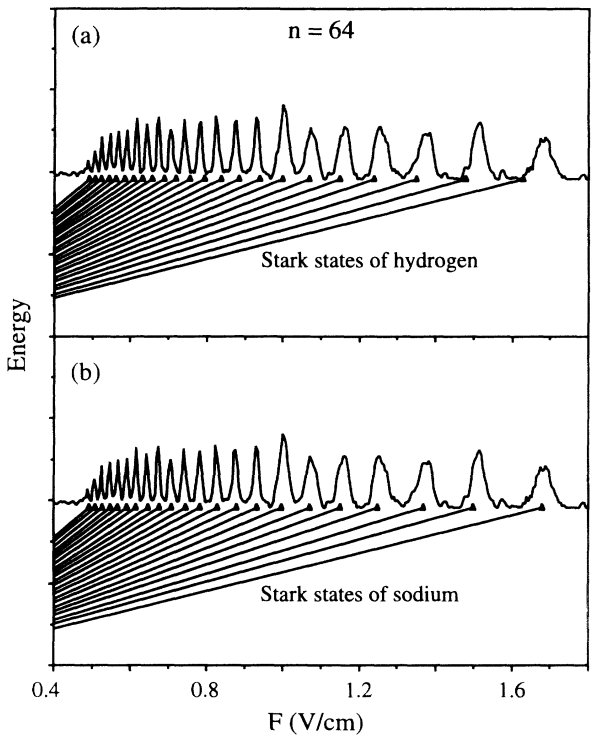

FIG. 5. F spectrum of the $n=64$ hydrogenic manifold of sodium acquired using the $10P(24)$ line of the CO_2 laser and the $12s\ ^2S$ intermediate state. Both panels show the same spectrum. (a) The Stark states are those of hydrogen $n=64$. (b) The Stark states are those of sodium $n=64$ calculated from the parameters measured in this work.

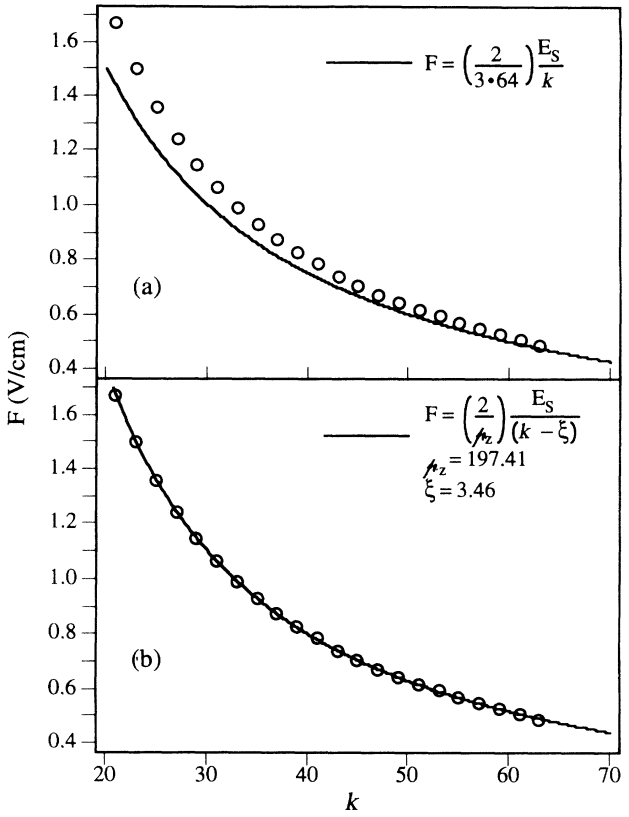

FIG. 6. Positions of peaks in the $n=64$ hydrogenic manifold of sodium taken from the F spectrum shown in Fig. 5. (a) The plotted curve is the displayed equation. It represents the predicted positions of the peaks for hydrogen atoms. (b) The plotted curve is the modified hydrogen equation displayed. The values of $\hbar_z$ and ξ were obtained by fitting the form of the curve to the data.

the z component of the permanent dipole moment. The ranges of parabolic quantum numbers for the Stark map in Fig. 5(a) are $41 \le n_1 \le 63$ and $0 \le n_2 \le 22$. To modify Eq. (17) so that it can apply to a hydrogenic manifold of sodium we replace k by $k-\xi$ and $3n$, the quantum of z component of dipole moment (QDM) for hydrogen, by an adjustable QDM, $\hbar_z$,

$$E_S(k,\xi,\hbar_z,F)=\tfrac{1}{2}\hbar_z(k-\xi)F\ . \tag{18}$$

We then fit the data to Eq. (18) and determine ξ and $\hbar_z$ for the $n=64$ manifold of sodium. Note that this technique ensures equal increments of $\hbar_z$ and thus equal spacing between adjacent Stark states at fixed F. The error limits on the determinations of ξ and $\hbar_z$ will, however, constitute a test of this assumption.

Figure 6 is a plot of the values of F at which peaks occur in Fig. 5 vs k. The curve in the top panel is simply a graph of Eq. (17). The curve in the bottom panel is a quasi-Newton fit of the peak positions to Eq. (18) from which ξ and $\hbar_z$ were determined to be 3.46 and 197.41, respectively. The value of the correlation coefficient for this fit, 0.999 94, suggests that indeed the assumption of constant increments of the QDM is valid, but that $\hbar_z$ is larger than p_z, the QDM for hydrogen, by roughly 3%. Using these parameters we construct a Stark map for the $n=64$ manifold of sodium as shown in Fig. 5(b). We note that unique assignments of k, n_1, and n_2 cannot be made for sodium because ξ is only unique mod2. We have chosen it so that n_1 and n_2 coincide with hydrogen quantum numbers.

The QDM obtained above is not only peculiar to the $n=64$ manifold, but also peculiar to the energy difference between the zero-field energy of the hydrogenic manifold and the three-photon energy. Careful inspection of accurate Stark maps for sodium [12] reveals the deviations from linear behavior that must occur for multielectron atoms. For example, as F increases, the blue Stark states of the hydrogenic manifold bend, more or less in unison, toward the abscissa, a result of perturbation by the nearest p state which, for sodium, lies above the hydrogenic manifold. Because δ_1 for sodium is substantial, 0.85, zero-field p states exhibit a quadratic Stark effect at fields well beyond those at which Stark states linked to states for which $l \ge 2$ begin to behave linearly. Eventually, as F increases, *all* quadratic Stark states behave linearly and join the hydrogenic manifold of states. As the F dependence of the (former) p state becomes linear, it repels the lower-lying blue hydrogenic states. The result is that ΔE_S changes slightly when this bending occurs, but the separations between adjacent Stark states remain nearly uniform for each value of F. Because we are limited to three-photon energies imposed

by the availability of CO_2 laser lines, we are unable to adjust the position on the Stark maps at which F spectra may be recorded. Therefore, it is difficult to systematically compare the QDM obtained for different hydrogenic manifolds. Nevertheless, from data acquired using several different CO_2 laser lines, as well as different intermediate state, it is our general observation that the QDM for sodium are roughly 1–5 % greater than for the corresponding manifolds of hydrogen.

It is interesting to examine the reason for the greater QDM in sodium in terms of the classical model. The permanent electric dipole moment of an electron in Keplerian orbit about a proton is a consequence of Kepler's second law, according to which the electron moves more slowly near apocenter than near pericenter [24]. The ionic core of the Rydberg atom provides an additional attractive potential, in this case proportional to $1/r^4$, which results from polarization of the core by the valence electron. This short-range perturbation to the Keplerian orbit causes the electronic orbital speed to increase near pericenter, but has little effect near apocenter. The result is an increase in the Keplerian electric dipole moment.

Using the value of ξ and $\not{\mu}_z$ derived from the data, we produce a Stark map of the $n=64$ manifold of sodium and compare it with the F spectrum. Figure 5(b) shows this sodium manifold together with the same spectrum shown in Fig. 5(a). As is clear, the predicted positions of the peaks match the data. This agreement is, of course, a consequence of the goodness of fit in the determinations of ξ and $\not{\mu}_z$.

We further explore the extent to which hydrogenic states of sodium behave as states of hydrogen by examining their responses to the rf field. In particular, we compare the spectral features with the predicted Floquet state absorption strengths for hydrogen [see Eq. (10)]. The data also illustrate the oscillatory behavior of the absorption strengths that results from the oscillatory behavior of the Bessel functions [28]. The simple expression for $|C_k|^2$ in Eq. (9) is in contrast to that for nonhydrogenic states, which is somewhat more complicated [19,29].

Examination of the relative absorption strengths for the sidebands of a given progenitor level, a dc Stark state, is best achieved for $\omega_S \gg \omega_0$. When this condition prevails, a single progenitor and several of its sidebands can be isolated from adjacent states as illustrated in Fig. 7, which is a Floquet-Stark diagram for hydrogen. To avoid the region of spaghetti we examined the $n=45$ manifold, for which there is a conveniently located line of the CO_2 laser, as shown in the figure. The results pertain to other manifolds in the range of fields for which the linear dc Stark effect occurs.

Figure 8 shows data for the $n=45$ manifold of sodium for values of $F \approx 9$ V/cm, $\omega_S \approx 1600$ MHz, acquired with $\omega_0 = 115$ MHz, as illustrated in Fig. 7. The shaded region in Fig. 7 corresponds to the approximate dc field over which the data have been acquired, approximate because this is a hydrogen diagram, not sodium. Figure 8a shows the F-spectrum with no rf field present, i.e., only excitation to the progenitor occurs. Figure 8(b) shows that excitation to the progenitor and several sideband states occurs when the rf field is turned on. For the spectrum in Fig. 8(c) the amplitude G was adjusted to a value, designated G_0, such that $J_0(p_z G_0/\hbar\omega)=0$, thus inhibiting absorption by the progenitor. Also shown in the figure are the squares of the Bessel functions that represent the predicted absorption strengths for states of hydrogen. As may be seen, agreement between the observed F spectra and the predicted intensities for hydrogen atoms is quite good, suggesting that under these conditions, the hydrogenic manifolds comprise states that behave as states of hydrogen. Moreover, because of this agreement, the vanishing of the transition moment provides a means of measuring rf field strengths with high precision [28].

We may probe the details of a Floquet-Stark map such as that shown schematically in Figs. 2(d) and 2(e), using our experimental technique. We use the $n=64$ hydrogenic manifold of sodium, which is accessed through $Na(12s\ ^2S)$ using the $10P(24)$ line of the CO_2 laser. Figure 9 shows three F spectra, each acquired at a different value of the rf amplitude G, as indicated in the figure; ω_0 was 400 MHz for all three spectra. The lowest one, acquired with $G=0$, serves as a reference because it contains

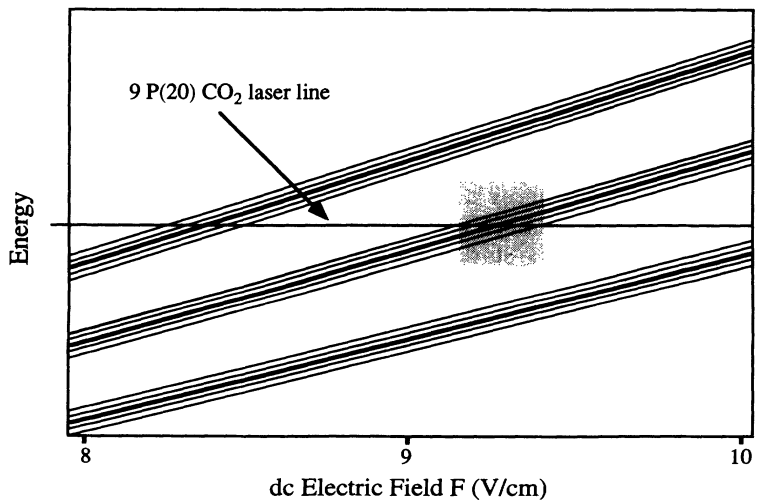

FIG. 7. Energy-level diagram of hydrogen Stark states in the $n=45$ manifold under the assumption that both a dc field F and an ac field $G\cos(\omega_0 t)$ are applied; $\omega_0 = 115$ MHz. The heavy lines are progenitor states, eigenstates of the time-independent Hamiltonian, while the lighter lines are sideband, or Floquet, states.

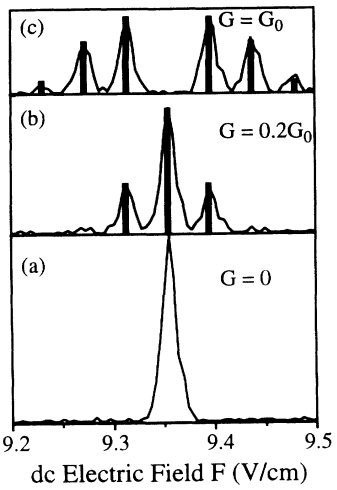

FIG. 8. F spectra acquired using the $9P(20)$ line of the CO_2 laser and the $10d\ ^2D_{5/2}$ intermediate state with $\omega_0=115$ MHz. The spectrum in (a) was acquired with no rf field present. The rf field strength was set to an arbitrary value to acquire the spectrum shown in (b). To acquire the data in (c) the amplitude G of the rf was adjusted to eliminate transitions to the progenitor state, as discussed in the text. The bars represent the predicted intensities according to Eq. (9).

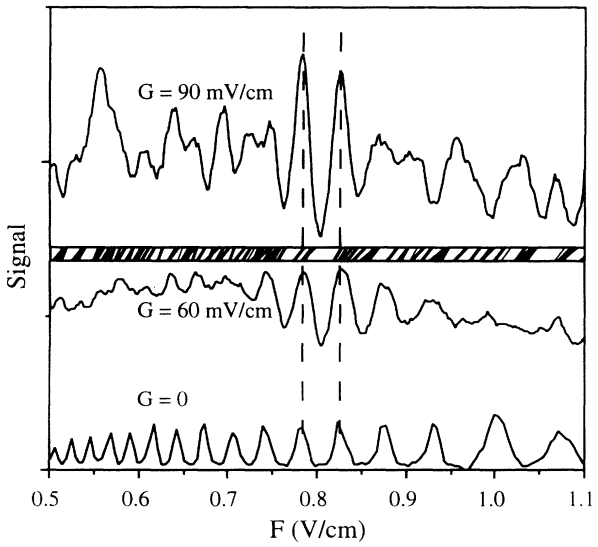

FIG. 9. Three F spectra of the $n=64$ hydrogenic manifold of sodium acquired using different values of the rf amplitude G. As the amplitude is increased, Floquet sidebands may be excited, except in the region of the Floquet-Stark map that contains gaps, as discussed in the text. The band between the two top F spectra is a slice from the Floquet-Stark map for the region near the three-photon energy. This band shows the density of Floquet states at the energy of this experiment. The dashed lines have been drawn to emphasize spectral features that are essentially unaltered by variations of G.

features resulting from excitation of progenitors only; it is the same spectrum shown in Fig. 5. At nonzero values of G, sidebands are excited, as seen in the other two spectra shown in Fig. 9. Included in this figure is a slice from the appropriate map at the three-photon energy [12]. This slice shows the density of available states as a function of F. The map from which this slice has been extracted is based on the Na($n=64$) parameters derived in this work; it was generated using six sidebands, three on each side of the progenitors.

The dashed lines in Fig. 9 enclose the gap in the density of states at $F=0.79$ V/cm, that corresponding to $2\omega_S=\omega_0$. For comparison with Fig. 2, which is a generic Floquet-Stark map for hydrogen atoms, $[\hbar\omega_0/3n)]=1.63$ V/cm for $n=64$ and $\hbar\omega_0=400$ MHz. It is seen that the two features bounding this gap in Fig. 9 remain essentially unchanged from spectrum to spectrum, a result of the absence of accessible states. Other gaps, arising from longer system periods, are present, but are more difficult to resolve experimentally. It is important to emphasize that the shapes and widths of the two peaks that surround the gap depend upon several factors. First, of course, is the instrumental resolution, which depends upon the uniformity of the fields as determined by the Stark plates [12–14,19]. More importantly, however, are the oscillatory behavior of the absorption strengths and the location of the three-photon energy on the Floquet-Stark map. Referring to the strip of Floquet-Stark map in Fig. 9, it is seen that absorption by any of the sidebands bordering the gap can occur. Since the absorption strength for each sideband depends upon the rf amplitude, few or many sidebands may contribute to the spectrum, depending on the value of G.

The location of the three-photon energy on the Floquet-Stark map also determines, to a large degree, the nature of the spectral features. This may be seen by inspection of Fig. 2(e). If, for example, the vertical position of the three-photon energy happened to coincide with the intersection point of the sidebands, then as F is scanned through this point, a very sharp peak, broadened only by instrumental resolution, would be observed. If, on the other hand, the three-photon energy crossed a gap, then a pair of peaks, each resulting from excitation to a myriad of sidebands bordering the gap, would be observed. This case is illustrated in Fig. 9 near $F=0.79$ V/cm. The closer the three-photon energy lies to the (vertical) midpoint between two sideband intersection points, the wider the gap in the spectrum.

The manifestation of the gaps in the F spectra of sodium is a consequence of the constant separation between adjacent linear dc Stark states at a given value of F. If this separation were not constant, then the structure of the Floquet-Stark map would differ from that shown in Figs. 2(d) and 2(e). Accordingly, ω_S would be different for each Stark state and commensurability would be impossible. Thus the effects of the gaps in F spectra for $G\neq 0$ confirm the near hydrogenic behavior of these states when subjected to an electric field, that is, the z component of the effective permanent electric dipole moment is quantized.

These F spectra illustrate other features of this atomic system. For example, irrespective of the gaps, the density of states must decrease with increasing F. The middle spectrum clearly shows this. On the other hand, the top spectrum actually has more features than the middle one. This is due to the combined effects of the density of states and the oscillating absorption probabilities. There is, however, little correlation between features in these two spectra, except for those near $F=0.79$ V/cm. In fact, there are a few instances where peaks occur in one spectrum at values of F for which minima occur in the other, e.g., $F=0.51$, 0.93, and 1.0 V/cm.

CONCLUSIONS

Classical and quantal descriptions of the responses of an atom to an external dc electric field and an external ac field of radio frequency have been presented. These descriptions have been used to understand the energy-level structure that results from simultaneous application of ac and dc electric fields to excited states of hydrogen and hydrogenic states of Rydberg atoms. This understanding has been used to develop Floquet spectroscopy, which, in conjunction with dc Stark spectroscopy, has been used to examine the degree to which hydrogenic states of sodium Rydberg atoms behave as states of hydrogen. As for hydrogen, it was found that the separation between adjacent Stark states within a given hydrogenic manifold is constant, although the separation depends upon the value of the dc field at which the measurement is made. This constant separation indicates that, as for hydrogen, the z component of the effective permanent electric dipole moment is quantized. It was found that the quanta of the electric dipole moment of hydrogenic states of sodium are consistently 1–5 % greater than those for corresponding states of hydrogen. The mechanism that causes this increase has been clarified with the aid of a classical model of the Rydberg atom. An empirical formula for these QDM's based on the hydrogen expression was used and found to fit accurately our measured Stark energies.

Absorption strengths for excitation to sidebands of hydrogenic states of sodium that result from imposition of the rf field were found to be in remarkable agreement with those calculated for sidebands of excited states of hydrogen. Moreover, in contrast to the effect observed for nonhydrogenic states, the field-free (nearly) degenerate hydrogenic states exhibited no ac Stark shift. By adjusting the rf amplitude and frequency it was possible to force the transition moment to a given state to vanish, thus providing a means for accurately measuring ac field strengths.

ACKNOWLEDGMENTS

The authors would like to thank Professor Peter M. Koch for helpful comments. This work was supported by the National Science Foundation and the University of Missouri Research Board.

[1] S. H. Autler and C. H. Townes, Phys. Rev. **100**, 703 (1955).
[2] See, for example, T. Zuo, S. Chelkowski, and A. D. Bandrauk, Phys. Rev. A **48**, 3837 (1993).
[3] P. M. Koch, J. Phys. (Paris) Colloq. **43**, C2-187 (1982).
[4] T. F. Gallagher, *Rydberg Atoms* (Cambridge University Press, Cambridge, England, 1994).
[5] T. Helgaker and I. Tomashevsky, Phys. Scr. **46**, 354 (1992).
[6] D. Humm and M. Nayfeh, Phys. Rev. A **40**, 3727 (1989).
[7] M. Stevens and B. Sundaram, Phys. Rev. A **36**, 417 (1987).
[8] J. Leopold and D. Richards, J. Phys. B **20**, 2369 (1987).
[9] R. Jensen, Phys. Rev. Lett. **54**, 2057 (1985).
[10] J. E. Bayfield and P. M. Koch, Phys. Rev. Lett. **33**, 258 (1974).
[11] For a textbook discussion of microwave ionization and recent references, see H. Friedrich, *Theoretical Atomic Physics* (Springer-Verlag, Berlin, 1990).
[12] M. Ciocca, C. E. Burkhardt, J. J. Leventhal, and T. Bergeman, Phys. Rev. A **45**, 4720 (1992).
[13] P. McNicholl, T. Bergeman, and H. J. Metcalf, Phys. Rev. A **37**, 3302 (1988).
[14] D.-H. Yang, D. Lieberman, P. van der Straten, T. Bergeman, and J. J. Metcalf, Phys. Rev. A **40**, 5026 (1989).
[15] D. Keppner, M. G. Littman, and M. L. Zimmerman, in *Rydberg States of Atoms and Molecules*, edited by R. F. Stebbings and F. B. Dunning (Cambridge University Press, Cambridge, England, 1983).
[16] See, for example, J. Mathews and R. L. Walker, *Mathematical Methods of Physics*, 2nd ed. (Benjamin/Cummings, Menlo Park, CA, 1964).
[17] T. F. Gallagher, C. R. Mahon, P. Pillet, Panming Fu, and J. B. Newman, Phys. Rev. A **39**, 4545 (1989), and references cited therein.
[18] See, for example, F. Arfken, *Mathematical Methods for Physicists*, 3rd ed. (Academic, Orlando, 1985).
[19] Y. Zhang, M. Ciocca, L.-W. He, C. E. Burkhardt, and J. J. Leventhal, Phys. Rev. A **50**, 1101 (1994).
[20] T. P. Hezel, C. E. Burkhardt, M. Ciocca, L.-W. He, and J. J. Leventhal, Am. J. Phys. **60**, 329 (1992).
[21] R. R. Freeman and D. Kleppner, Phys. Rev. A **14**, 1614 (1976).
[22] W. van de Water, S. Yoakum, T. van Leeuwen, B. E. Sauer, L. Moorman, E. J. Galvez, D. R. Mariani, and P. M. Koch, Phys. Rev. A **42**, 572 (1990).
[23] B. E. Sauer, S. Yoakum, L. Moorman, P. M. Koch, D. Richards, and P. A. Dando, Phys. Rev. Lett. **68**, 468 (1992).
[24] T. P. Hezel, C. E. Burkhardt, M. Ciocca, and J. J. Leventhal, Am. J. Phys. **60**, 324 (1992).
[25] I. C. Percival and D. Richards, J. Phys. B **12**, 2051 (1979).
[26] M. Tabor, *Chaos and Integrability in Nonlinear Dynamics* (Wiley, New York, 1989).
[27] L. E. Reichl, *The Transition to Chaos* (Springer-Verlag, New York, 1992).
[28] M. Gatzke, M. C. Baruch, R. B. Watkins, and T. F. Gallagher, Phys. Rev. A **48**, 4742 (1993).
[29] P. Pillet, R. Kachru, N. H. Tran, W. W. Smith, and T. F. Gallagher, Phys. Rev. A **36**, 1132 (1987).

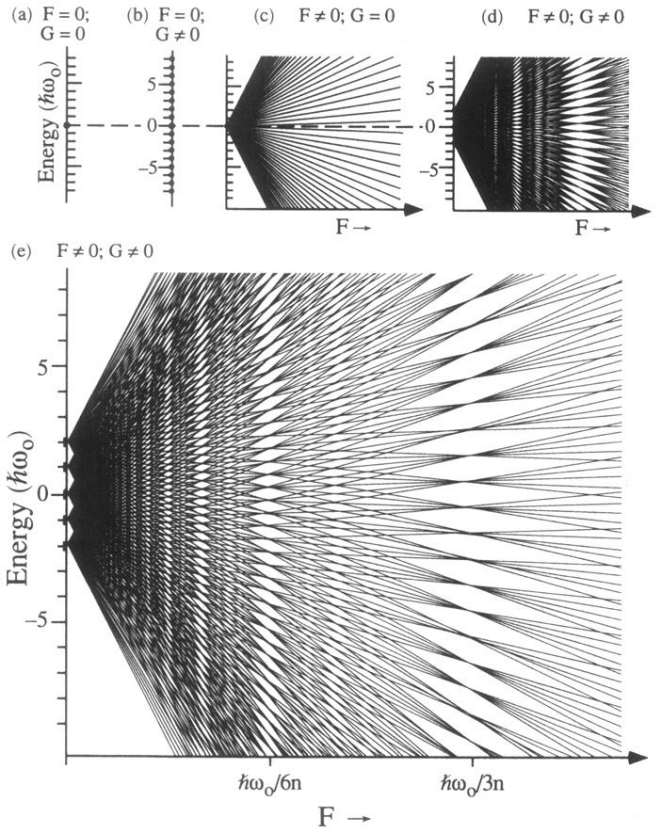

FIG. 2. Schematic energy-level diagram showing the splitting of a degenerate hydrogenic state under application of dc and ac electric fields for the cases indicated; (e) is an enlarged version of (d) to show detail. F is in a.u. provided $\hbar\omega_0$ is in a.u. The dashed line though the degenerate field-free progenitor states in (a)–(d) emphasizes the fact that these states do not shift energy upon application of the ac field.

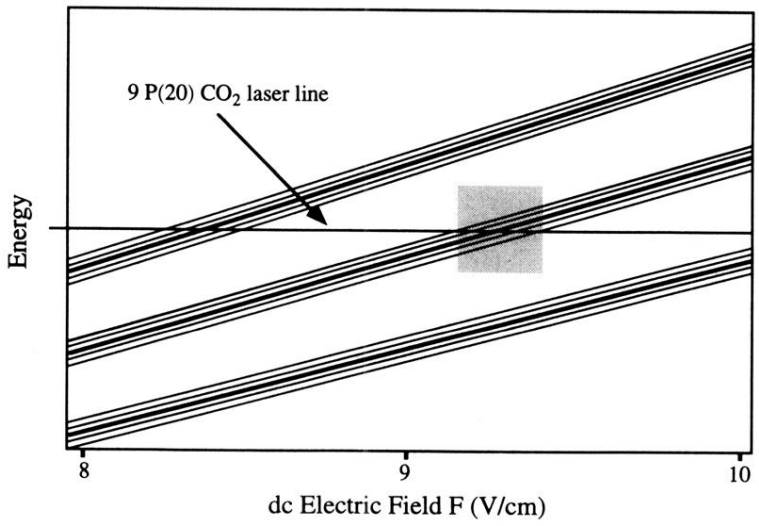

FIG. 7. Energy-level diagram of hydrogen Stark states in the $n=45$ manifold under the assumption that both a dc field F and an ac field $G\cos(\omega_0 t)$ are applied; $\omega_0=115$ MHz. The heavy lines are progenitor states, eigenstates of the time-independent Hamiltonian, while the lighter lines are sideband, or Floquet, states.